# Understanding the Shape of Sickled Red Cells

Garrott W. Christoph, James Hofrichter, and William A. Eaton
Laboratory of Chemical Physics, National Institute of Diabetes and Digestive and Kidney Diseases, National Institutes of Health, Bethesda, Maryland

ABSTRACT To understand the physical basis of the wide variety of shapes of deoxygenated red cells from patients with sickle cell anemia, we have measured the formation rate and volume distribution of the birefringent domains of hemoglobin S fibers. We find that the domain formation rate depends on the ~80th power of the protein concentration, compared to ~40th power for the concentration dependence of the reciprocal of the delay time that precedes fiber formation. These remarkably high concentration dependences, as well as the exponential distribution of domain volumes, can be explained by the previously proposed double nucleation model in which homogeneous nucleation of a single fiber triggers the formation of an entire domain via heterogeneous nucleation and growth. The enormous sensitivity of the domain formation rate to intracellular hemoglobin S concentration explains the variable cell morphology and why rapid polymerization results in cells that do not appear sickled at all.

## INTRODUCTION

An increasing number of human diseases are now thought to be caused by abnormal peptide or protein aggregation, most notably Alzheimer's, Parkinson's, and prion diseases (Dobson, 2003). The amyloid aggregates found in these disorders contain fibers in a variety of arrangements, including partially ordered, birefringent arrays (Sipe and Cohen, 2000). A similar phenomenon occurs in sickle cell anemia, the most well understood of the protein aggregation diseases (Eaton and Hofrichter, 1987, 1990; Bunn, 1997). Sickle cell anemia is caused by a mutation from a glutamate to a valine in the beta chain of the hemoglobin molecule (Pauling et al., 1949; Ingram, 1957). The change from a charged to a neutral, hydrophobic amino acid creates a sticky patch on the molecular surface that causes aggregation upon deoxygenation. The aggregates are polymers of hemoglobin S molecules that consist of 14-stranded fibers assembled into birefringent domains (Dykes et al., 1978; Eaton and Hofrichter, 1990; Cretegny and Edelstein, 1993; Watowich et al., 1993). These fiber domains distort ('sickle') and decrease the flexibility of the red cell necessary for its passage though the narrow vessels in the tissues, potentially causing occlusion of blood flow, organ damage, and the pain crises characteristic of the disease (Fig. 1).

Kinetics plays an extremely important role in the pathophysiology (Hofrichter et al., 1974; Eaton and Hofrichter, 1987). If polymerization were sufficiently rapid to reach equilibrium, almost all cells would contain fibers and be much less deformable at the oxygen pressure of the tissues (Mozzarelli et al., 1987). However, widespread blockage of the circulation is avoided, and the disease survivable, because of the highly unusual kinetics of polymerization. They are characterized by a marked delay period before any fibers can be detected (Fig. 1), with a duration that depends inversely on an extraordinarily high power (up to 40th) of the initial protein concentration (Hofrichter et al., 1974; Eaton and Hofrichter, 1990). Consequently, in each roundtrip from the lungs to the tissues the vast majority of cells escape the narrow vessels of the microcirculation before any significant polymerization has begun (Mozzarelli et al., 1987) (Fig. 1 *B*). If fibers do form, the cells undergo varying degrees of distortion that depend on the rate of deoxygenation (Sherman, 1940; Eaton and Hofrichter, 1990) and on the intracellular protein concentration (Corbett et al., 1995). To understand the physical basis of this connection, we have measured the distribution of domain volumes in gels formed with known delay times, from which we have also determined the rate of domain formation.

## MATERIALS AND METHODS

Hemoglobin S from a patient with homozygous sickle cell disease was purified by DEAE-Sephacel chromatography, concentrated by vacuum dialysis, and buffered to pH 7.2 with 0.15 M potassium phosphate. After deoxygenation sodium dithionite was added to a final concentration of 50 mM to remove any residual oxygen and layers of cold solution were sealed under nitrogen between a slide and coverslip that was thermostated with a thermoelectric controller in a copper housing on the stage of a microspectrophotmeter. The thickness of the layers, which varied between 5 and 60 microns, were determined from the known concentration and optical density.

Kinetics of polymerization were measured after an ~30 s temperature jump from 276 K to final temperatures between 289 K and 308 K by continuously monitoring the birefringence from the intensity of a 458-nm argon ion laser transmitted through the sample placed between crossed Glan-Thompson calcite linear polarizers. The delay time for each progress curve was taken as the time at which the maximal slope of the progress curve intersects with the time axis.

Images of the polymerized sample between crossed linear polarizers at various magnifications between 25× and 400× were recorded with a video

*Submitted August 17, 2004, and accepted for publication October 29, 2004.*

Address reprint requests to William A. Eaton, Laboratory of Chemical Physics, Bldg. 5, Rm. 104, National Institutes of Health, Bethesda, MD 20892-0520. Tel.: 301-496-6030; Fax: 301-496-0825; E-mail: eaton@helix.nih.gov.



0006-3495/05/02/1371/06 $2.00

doi: 10.1529/biophysj.104.051250

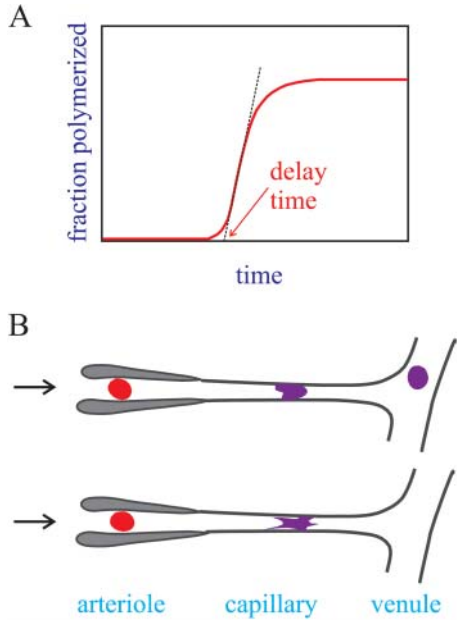


FIGURE 1 Delay time of hemoglobin S polymerization and transit of red cells though the microcirculation (adapted from Eaton and Hofrichter, 1995). (*A*) Kinetic progress curve for the polymerization of hemoglobin S. The delay time is determined by the hemoglobin S concentration and the rate and extent of deoxygenation. (*B*) Simplified schematic of microcirculation showing a cell passing from the arteriole to the venous circulation. (*Top*) A red cell deforms as it passes through a capillary and escapes into the large vessels on the venous side without intracellular polymerization because the transit time is shorter than the delay time. (*Bottom*) The delay time is shorter than the capillary transit time, and polymerization occurs while the cell is in the capillary, with the possibility of blocking the circulation. A small reduction in the intracellular sickle hemoglobin concentration will markedly increase the delay time and should therefore be therapeutic (Hofrichter et al., 1974; Sunshine et al., 1978; Eaton and Hofrichter, 1987). This dynamical description of the pathophysiology explains why hydroxyurea stimulation of F-cell production, in which sickle hemoglobin is diluted by replacement with fetal hemoglobin, has proven to be effective in double blind clinical trials (Charache et al., 1995; Eaton and Hofrichter, 1995; Bridges et al., 1996; Bunn, 1997; Steinberg and Brugnara, 2003). It also explains why preventing concentration increases from cellular dehydration due to the damage to membrane channels appears to be a promising approach to therapy (Steinberg and Brugnara, 2003).

camera. Domains were defined as having four lobes of light transmission with a central region of extinction, as observed for the largest domains. A range of magnifications was employed to insure that smaller domains were counted. This method of analysis included more than ~75% of the area of the sample. The area of each domain was determined by two, roughly perpendicular diameters. The domain volume was then calculated by approximating the domain as a right circular cylinder with volume $V = \pi\langle r\rangle^2 t$, where $t$ is the sample thickness and the radius $\langle r\rangle$ is determined from the average of the two measured diameters (Fig. 2).

## RESULTS AND DISCUSSION

Fig. 3 shows the time course of polymerization at different concentrations of fully deoxygenated hemoglobin S and optical birefringence micrographs of the resulting gels. (In contrast to amyloid, where an extrinsic chromophore such as

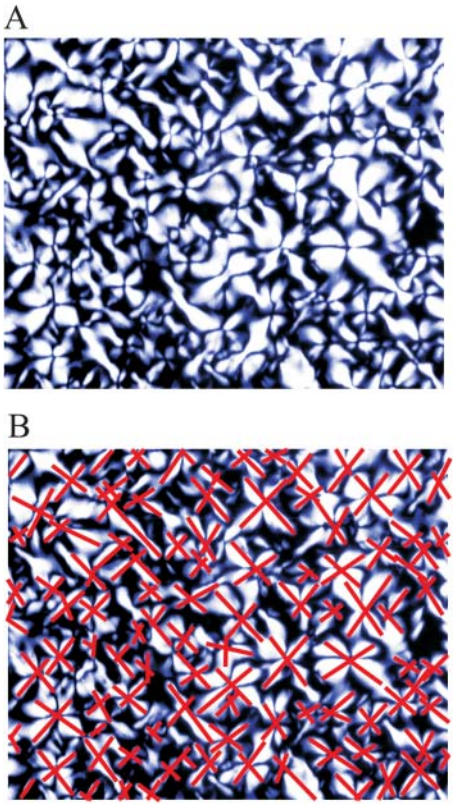


FIGURE 2 Counting domains. (*A*) Optical micrograph (image size 1.26 × 1.00 mm) of gel formed with a delay time of 52 seconds. (*B*) Same micrograph with lines indicating the domain diameters from which the domain volume was calculated.

Congo red must be bound to produce readily observable birefringence, the birefringence of sickle hemoglobin gels is easily visualized because of the intense absorption and high anisotropy of the intrinsic heme chromophore (Hofrichter et al., 1973; Eaton and Hofrichter, 1981). As the delay time increases with decreasing concentration or temperature there is a marked decrease in the density of domains. Fig. 4 *A* shows that the delay times and mean volumes at all concentrations and temperatures are strongly correlated, indicating that the morphology of the gel is determined by the kinetics of its formation. An interesting property of the gels is that they have a very similar appearance when magnified or demagnified to the same mean diameter for individual domains. To make this comparison quantitative, the distribution of domain volumes obtained from each experiment was scaled by the average domain volume for that experiment, $\langle V\rangle$. The distribution of $V/\langle V\rangle$, calculated from all of the normalized data is shown in Fig. 4 *B*, as well as distributions obtained from subsets of the experiments with largest (long delay times) and smallest (short delay times) domain volumes. The distributions are very similar, exhibiting a peak at small volumes and an exponential decay. The similar shapes of the volume distributions suggests that domains of all sizes have the same structure (i.e., organization of fibers) and form by the

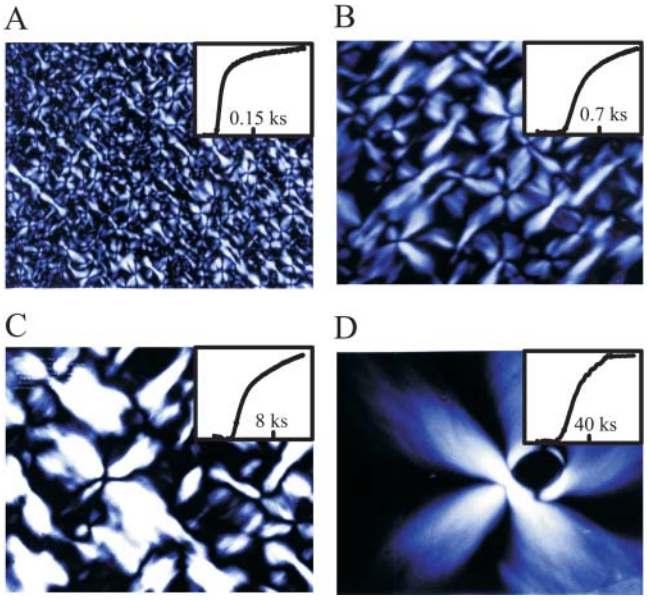


FIGURE 3 Optical birefringence micrographs of gels and kinetic progress curves. The inset shows the square root of the light intensity transmitted between crossed linear polarizers (proportional to the fraction polymerized) as a function of time after a temperature jump from 276 K to 303 K. The delay times and initial hemoglobin S concentrations in panels *A*, *B*, *C*, and *D* are (38 s, 4.08 mM), (360 s, 3.98 mM), (3,700 s, 3.58 mM), and (24,000 s, 3.50 mM), respectively. In each case, the image size is 1.16 × 0.93 mm.

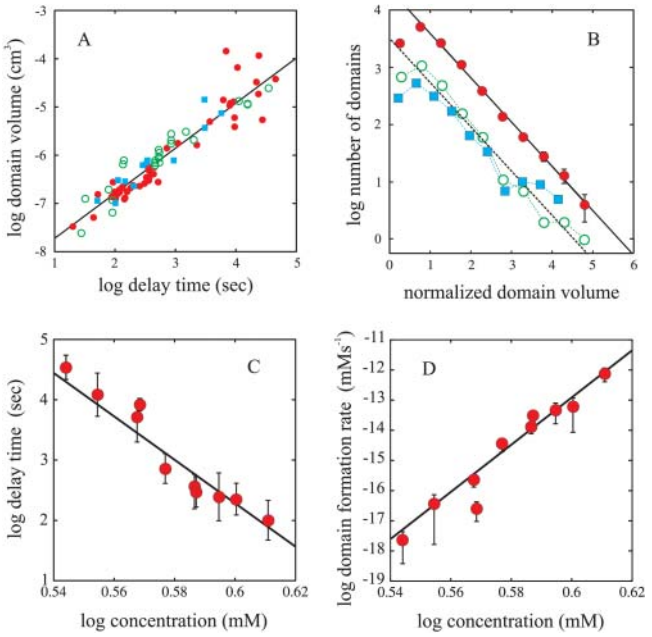


FIGURE 4 Domain volumes and concentration dependence of delay time and domain formation rate. (*A*) The mean domain volume from each experiment is shown as a function of the delay time. (●) Data obtained at 303 K at varying Hb S concentrations. (○) Data obtained at 296 K at different Hb S concentrations. (■) Data obtained at a Hb S concentration of 4.02 mM at temperatures between 287 K and 308 K. (*B*) Distribution of normalized domain volumes for all of the data (*red solid circles*), the distribution for the subset of samples with shortest delay times (2498 domains) (*open green circles*), and the distribution for the subset of samples with the longest delay times (1437 domains) (*cyan squares*). (*C*) Delay time versus initial protein concentration. The slope from the linear least squares fit is −41 ± 4. (*D*) Domain formation rate versus initial protein concentration: slope = 80 ± 7.

same mechanism. The exponential decay in the volume distribution is characteristic of objects that are randomly distributed in space. This probability distribution of points at particle density $n$ was treated by Chandrasekhar (1943). The distribution of nearest neighbor distances is given by

$$w(r)dr = 4\pi r^2 \exp\left(-\frac{4\pi r^3 n}{3}\right)dr,$$

where $w(r)dr$ is the probability that the nearest neighbor is between $r$ and $r + dr$. If a sphere with a radius that is half the distance to its nearest neighbor is assigned to each particle, the distribution of volumes associated with these particles is

$$w(V)dV = 8n\exp(-8nV)dV.$$

Whereas the spheres constructed in this way would not fill space, this simple calculation suggests that the exponential tail of the distribution could be explained by arguing that observable gel domains are simply a set of objects positioned randomly in space.

Linear least squares fits show that the concentration dependence of the delay time is 41 ($\pm$ 4)$^{st}$ power (Fig. 4 *C*), very similar to what has been observed in previous studies in this range of delay times and temperatures (42 (Hofrichter et al., 1976), 33 ± 4 (Sunshine et al., 1979), and 38 ± 2 (Ferrone et al., 1985b)). The observation of an extremely high concentration dependence to the observed domain density also indicates that the rate of domain formation is highly concentration dependent. To calculate this rate, we assume that it is constant during the delay period because there is no evidence of any decrease in monomer concentration. After the initial detection of birefringence, visual observations showed that the domain density does not change, consistent with the expectation that the rate would shut down as soon as significant monomer depletion begins because of its high concentration dependence. The domain formation rate can then simply be obtained from the final concentration of domains divided by the delay time. Fig. 4 *D* shows that the concentration dependence of the domain formation rate is an astonishing 80 ($\pm$7)$^{th}$ power (a 15% increase in sickle hemoglobin concentration increases the domain formation rate by almost five orders of magnitude).

Our results can be understood in terms of the double nucleation model for fiber formation (Ferrone et al., 1980, 1985a, 2002; Eaton and Hofrichter, 1990; Samuel et al., 1990; Briehl, 1995; Cao and Ferrone, 1997; Vaiana et al., 2003; Galkin and Vekilov, 2004). According to this model nucleation of a single fiber at random locations in the solution (homogeneous nucleation) triggers the autocatalytic formation of a large number of additional fibers via secondary

nucleation on the surface of existing ones (heterogeneous nucleation). Heterogeneous nucleation and growth produce an exponentially increasing amount of polymer with time, and therefore a delay period before a sufficient amount is formed to be detected. Both homogeneous and heterogeneous nucleation are highly concentration dependent because a large number of molecules must assemble to form a critical nucleus and because of changes in the effective thermodynamic concentration (activity) arising from molecular crowding in these concentrated protein solutions. The homogeneous nucleation rate has been directly measured from the distribution of delay times observed in repetitive experiments on small sample volumes. The distribution results from stochastic fluctuations in the time at which a single homogeneous nucleus molecule forms (Ferrone et al., 1980; Hofrichter, 1986; Szabo, 1988; Cao and Ferrone, 1996, 1997). For long delay times, in which no more than one nucleus is formed in the observation volume, the distribution is exponential and the decay gives the homogeneous nucleation rate directly. Szabo has shown how to extract the nucleation rate in the more complex situation when more than one nucleus is formed in the observation volume (Szabo, 1988).

A 60 $(\pm 10)^{\text{th}}$ power concentration dependence for the homogeneous nucleation rate was determined in a concentration range slightly higher than that employed in the present experiments (Ivanova et al., 2000). We find a comparable extraordinarily high power for the concentration dependence of the domain formation rate ($80 \pm 7$), with about twice the exponent observed for the delay time ($41 \pm 4$). (Both the homogeneous and heterogeneous nucleation rates depend on concentration to a power that is the size of their critical nuclei, i.e., $c^{i*}$ and $c^{j*}$, respectively. The inverse delay time depends primarily on the square root of the heterogeneous nucleation rate, i.e., on $c^{j*/2}$. In the concentration range of our experiments $i* \approx j*$ (Ferrone et al., 1985a), explaining the twofold higher concentration dependence of the homogeneous nucleation rate (Cao and Ferrone, 1996).

These results provide strong evidence that homogeneous nucleation of a single fiber is the rate-limiting process in forming a domain and triggers its growth via heterogeneous nucleation and fiber elongation (Ferrone et al., 1985a). Moreover, the random location of domains demonstrated by the exponential volume distribution is consistent with the underlying assumption of the double nucleation model that homogeneous nucleation occurs at random positions in the solution.

One possible caveat is that the absolute domain formation rate is more than 10-fold smaller than the homogeneous nucleation rate determined from delay time distributions (Hofrichter, 1986; Szabo, 1988; Cao and Ferrone, 1996, 1997; Ivanova et al., 2000). Such a difference is predicted by the double nucleation mechanism. The amount of polymer associated with each nucleation event increases exponentially via heterogeneous nucleation and growth. Since polymers grow linearly with time (Samuel et al., 1990), and since the maximum dimension of the domain is limited by the length of the longest fiber, the polymer density of the growing domain also increases exponentially. Consequently, the amount of polymerized hemoglobin S associated with nuclei that form late in the delay time is much smaller than that associated with earlier homogeneous nucleation events, with the result that they do not contribute significantly to the birefringence pattern. However, since the structure of gels is independent of domain density, as evidenced by the normalized volume distributions (Fig. 4 *B*), the fraction of undetected domains should be approximately independent of the delay time, and therefore should not significantly affect the relative domain formation rates.

Our results provide the key to explaining the wide range of shapes observed for red cells containing polymerized hemoglobin S. Sherman (1940) first showed that the shape of the red cell depends on the rate of deoxygenation (Fig. 5). (Sherman's experiments were influential in attracting Linus Pauling to think about sickle cell disease in the 1940s (Pauling et al., 1949; Eaton, 2003).) Since the nucleation rate varies with the supersaturation, which is the ratio of the total protein concentration to the equilibrium solubility (Hofrichter et al., 1976), the domain formation rate depends on the rate of the solubility decrease resulting from the decreasing oxygen pressure. Rapid deoxygenation corresponds to rapidly attaining a high supersaturation, and is therefore analogous to a high protein concentration in the experiments described above. The optical birefringence micrographs in Fig. 5 show that not only the morphology, but also the birefringence patterns of cells depend on the deoxygenation rate. Slow deoxygenation results in a single fiber domain that initially grows in one general direction (Basak et al., 1988; Samuel et al., 1990), with the classic sickled shape resulting from oblique alignment of adjacent fibers through interactions of their helical surfaces (Edelstein and Crepeau, 1979). In contrast, rapid deoxygenation produces cells that do not appear sickled at all, having a nearly normal biconcave disc shape, even though the cells are filled with multiple domains of polymerized hemoglobin as is evident from the birefringence pattern (Fig. 5 *E*). When cells are fractionated according to their intracellular hemoglobin concentration and deoxygenated at the same rate, the number of domains observed by linear dichroism increases with increasing concentration, consistent with the above analysis (Corbett et al., 1995).

Overall, the results on domain formation in hemoglobin S gels from this study provide strong support for the conclusion that the rate of homogeneous nucleation determines the density of fiber domains, and therefore the shape of the cell, as originally proposed by Ferrone et al. on the basis of theoretical arguments (Ferrone et al., 1985a; Eaton and Hofrichter, 1987). Our results suggest that it would be important to investigate the rheological properties of gels containing the same total amount of polymerized hemoglobin, but with

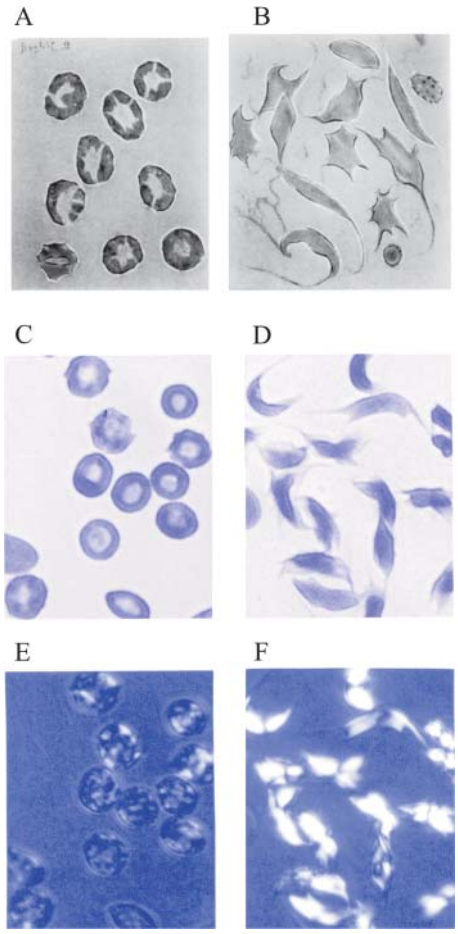


FIGURE 5 Optical micrographs of rapidly (seconds) *(panels A, C,* and *E)* and slowly (hours) (*panels B, D,* and *F*) deoxygenated sickle red cells. Panels *A* and *B* reproduced from Sherman (1940); panels *C–F* reproduced from Eaton and Hofrichter (1990). The micrographs of the cells in panels *C* and *D*, obtained with 430 nm linearly polarized light oriented horizontally, show greater absorption for cells with the polarization vector perpendicular to their long axis. The micrographs in panels *E* and *F* were taken with 450 nm light with the cells between crossed linear polarizers.

different domain densities because of their kinetic history. Such experiments on cells may lead to an understanding of the yet-to-be explored relative roles of cellular distortion and deformability in the mechanism of vaso-occlusion.

We thank Frank A. Ferrone and Attila Szabo for helpful discussion.

## REFERENCES

Basak, S., F. A. Ferrone, and J. T. Wang. 1988. Kinetics of domain formation by sickle hemoglobin polymers. *Biophys. J.* 54:829–843.

Bridges, K. R., G. D. Barabino, C. Brugnara, M. Cho, G. W. Christoph, G. Dover, B. Ewenstein, D. E. Golan, C. R. G. Guttmann, J. Hofrichter, R. V. Mulkern, B. Zhang, and W. A. Eaton. 1996. A multiparameter analysis of sickle erythrocytes in patients undergoing hydroxyurea therapy. *Blood.* 88:4701–4711.

Briehl, R. W. 1995. Nucleation, fiber growth and melting, and domain formation and structure in sickle cell hemoglobin gels. *J. Mol. Biol.* 245:710–723.

Bunn, H. F. 1997. Mechanisms of disease–pathogenesis and treatment of sickle cell disease. *N. Engl. J. Med.* 337:762–769.

Cao, Z. Q., and F. A. Ferrone. 1996. A 50th order reaction predicted and observed for sickle hemoglobin nucleation. *J. Mol. Biol.* 256:219–222.

Cao, Z. Q., and F. A. Ferrone. 1997. Homogeneous nucleation in sickle hemoglobin: Stochastic measurements with a parallel method. *Biophys. J.* 72:343–352.

Chandrasekhar, S. 1943. Stochastic problems in physics and astronomy. *Rev. Mod. Phys.* 15:1–89.

Charache, S., M. L. Perrin, R. D. Morre, G. J. Dover, F. B. Barton, S. V. Eckert, R. P. McMahon, and D. R. Bonds. 1995. Effect of hydroxyurea on the frequency of painful crises in sickle cell anemia. *N. Engl. J. Med.* 332:1317–1322.

Corbett, J. D., W. E. Mickols, and M. F. Maestre. 1995. Effect of hemoglobin concentration on nucleation and polymer formation in sickled red blood cells. *J. Biol. Chem.* 270:2708–2715.

Cretegny, I., and S. J. Edelstein. 1993. Double strand packing in hemoglobin-S fibers. *J. Mol. Biol.* 230:733–738.

Dobson, C. M. 2003. Protein folding and misfolding. *Nature.* 426:884–890.

Dykes, G. W., R. H. Crepeau, and S. J. Edelstein. 1978. Three-dimensional reconstruction of the fibres of sickle cell haemoglobin. *Nature.* 272:506–510.

Eaton, W. A. 2003. Linus Pauling and sickle cell disease. *Biophys. Chem.* 100:109–116.

Eaton, W. A., and J. Hofrichter. 1981. Polarized absorption and linear dichroism spectroscopy of hemoglobin. *Methods Enzymol.* 76:175–261.

Eaton, W. A., and J. Hofrichter. 1987. Hemoglobin S gelation and sickle cell disease. *Blood.* 70:1245–1266.

Eaton, W. A., and J. Hofrichter. 1990. Sickle cell hemoglobin polymerization. *Adv. Protein. Chem.* 40:63–279.

Eaton, W. A., and J. Hofrichter. 1995. The biophysics of sickle cell hydroxyurea therapy. *Science.* 268:1142–1143.

Edelstein, S. J., and R. H. Crepeau. 1979. Oblique alignment of hemoglobin-S fibers in sickled cells. *J. Mol. Biol.* 134:851–855.

Ferrone, F. A., J. Hofrichter, and W. A. Eaton. 1985a. Kinetics of sickle hemoglobin polymerization II. A double nucleation mechanism. *J. Mol. Biol.* 183:611–631.

Ferrone, F. A., J. Hofrichter, and W. A. Eaton. 1985b. Kinetics of sickle hemoglobin polymerization; I. Studies using temperature jump and laser photolysis techniques. *J. Mol. Biol.* 183:591–610.

Ferrone, F. A., J. Hofrichter, H. R. Sunshine, and W. A. Eaton. 1980. Kinetic studies on photolysis induced gelation of sickle cell hemoglobin suggest a new mechanism. *Biophys. J.* 32:361–377.

Ferrone, F. A., M. Ivanova, and R. Jasuja. 2002. Heterogeneous nucleation and crowding in sickle hemoglobin: An analytic approach. *Biophys. J.* 82:399–406.

Galkin, O., and P. G. Vekilov. 2004. Mechanisms of homogeneous nucleation of polymers of sickle cell anemia hemoglobin in deoxy state. *J. Mol. Biol.* 336:43–59.

Hofrichter, J. 1986. Kinetics of sickle hemoglobin polymerization. III. Nucleation rates determined from stochastic fluctuations in polymerization progress curves. *J. Mol. Biol.* 189:553–571.

Hofrichter, J., D. G. Hendricker, and W. A. Eaton. 1973. Structure of hemoglobin S fibers: optical determination of the molecular orientation in sickled red cells. *Proc. Natl. Acad. Sci. USA.* 70:3604–3608.

Hofrichter, J., P. D. Ross, and W. A. Eaton. 1974. Kinetics and mechanism of deoxyhemoglobin S gelation. A new approach to understanding sickle cell disease. *Proc. Natl. Acad. Sci. USA.* 71:4864–4868.

Hofrichter, J., P. D. Ross, and W. A. Eaton. 1976. Supersaturation in sickle cell hemoglobin solutions. *Proc. Natl. Acad. Sci. USA.* 73:3034–3039.

Ingram, V. M. 1957. Gene mutations in human hemoglobin: the chemical difference between normal and sickle cell hemoglobin. *Nature.* 180:326–328.

Ivanova, M., R. Jasuja, S. Kwong, R. W. Briehl, and F. A. Ferrone. 2000. Nonideality and the nucleation of sickle hemoglobin. *Biophys. J.* 79: 1016–1022.

Mozzarelli, A., J. Hofrichter, and W. A. Eaton. 1987. Delay time of hemoglobin-S polymerization prevents most cells from sickling in vivo. *Science.* 237:500–506.

Pauling, L., H. A. Itano, S. J. Singer, and I. C. Wells. 1949. Sickle cell anemia, a molecular disease. *Science.* 110:543–548.

Samuel, R. E., E. D. Salmon, and R. W. Briehl. 1990. Nucleation and growth of fibres and gel formation in sickle cell hemoglobin. *Nature.* 345:833–835.

Sherman, I. J. 1940. The sickling phenomenon, with special reference to the differentiation of sickle cell anemia from sickle cell trait. *Bull. Johns Hopkins Hospital.* 67:309–324.

Sipe, J. D., and A. S. Cohen. 2000. Review: history of the amyloid fibril. *J. Struct. Biol.* 130:88–98.

Steinberg, M. H., and C. Brugnara. 2003. Pathophysiological-based approaches to treatment of sickle cell disease. *Annu. Rev. Med.* 54:89–112.

Sunshine, H. R., J. Hofrichter, and W. A. Eaton. 1978. Requirements for therapeutic inhibition of sickle hemoglobin gelation. *Nature.* 275:238–240.

Sunshine, H. R., J. Hofrichter, and W. A. Eaton. 1979. Gelation of sickle-cell hemoglobin in mixtures with normal adult and fetal hemoglobins. *J. Mol. Biol.* 133:435–467.

Szabo, A. 1988. Fluctuations in the polymerization of sickle hemoglobin—a simple analytic model. *J. Mol. Biol.* 199:539–542.

Vaiana, S. M., M. B. Palma-Vittorelli, and M. U. Palma. 2003. Time scale of protein aggregation dictated by liquid-liquid demixing. *Proteins.* 51:147–153.

Watowich, S. J., L. J. Gross, and R. Josephs. 1993. Analysis of the intermolecular contacts within sickle hemoglobin fibers - effect of site-specific substitutions, fiber pitch, and double-strand disorder. *J. Struct. Biol.* 111:161–179.